

# Occupancy and site distribution of europium in barium magnesium aluminate by $^{151}\text{Eu}$ Mössbauer spectroscopy

P. Boolchand

*Department of Electrical and Computer Engineering, University of Cincinnati, Cincinnati, Ohio 45223*

K. C. Mishra and M. Raukas

*Osram Sylvania, 71 Cherry Hill Drive, Beverly, Massachusetts 01915*

A. Ellens\*

*OSRAM GmbH, Research and Development, München, Germany*

P. C. Schmidt

*Darmstadt University of Technology, Darmstadt, Germany*

(Received 10 May 2002; published 31 October 2002)

$\text{BaMgAl}_{10}\text{O}_{17}:\text{Eu}^{2+}$  (BAM) is a commercial, blue emitting lamp phosphor activated by  $\text{Eu}^{2+}$ . It is usually assumed that the Eu ions substitute for Ba ions occupying the Beavers-Ross site in the  $\beta$ -alumina structure. We have investigated this phosphor with varying europium concentrations and different synthesis conditions using  $^{151}\text{Eu}$  Mössbauer spectroscopy. Analysis of the Mössbauer line shapes reveals a pentamodal (or higher) site distribution consisting of three  $\text{Eu}^{2+}$  sites, one (or two)  $\text{Eu}^{3+}$  site(s), and a mixed valent site whose isomer shift lies in between those for the divalent and trivalent ions. The observed quadrupole coupling constants for the divalent ions are larger than any other reported to date in any lattice. Based on calculations of the nuclear quadrupole coupling constants by a full potential band-structure method reported recently, the divalent sites are identified with occupancy of the Beavers-Ross, anti-Beavers-Ross, and mid-oxygen sites in the  $\beta$ -alumina structure. Oxidative degradation of the divalent ions due to the thermal treatment in air was also studied, and a preliminary analysis of how various sites evolve during this process is also presented.

DOI: 10.1103/PhysRevB.66.134429

PACS number(s): 76.80.+y, 78.55.Hx, 76.30.Kg, 61.72.Ji

## I. INTRODUCTION

Barium magnesium aluminate ( $\text{BaMgAl}_{10}\text{O}_{17}$ ) activated by europium ions, also known as BAM, is widely used as a blue emitting phosphor in various lighting applications. The  $4f^65d \rightarrow 4f^7$  transition of  $\text{Eu}^{2+}$  in this phosphor leads to an emission band that peaks near 450 nm. Together with the red emitting phosphor,  $\text{Y}_2\text{O}_3:\text{Eu}^{3+}$  and a green emitting phosphor such as  $\text{LaPO}_4:\text{Ce}^{3+}$  and  $\text{Tb}^{3+}$ , it yields a white emitting blend for fluorescent lamps with a high color rendering index. In comparison to the red and green emitting phosphors in the triblend, BAM is relatively unstable with respect to temperature- and UV-induced degradation processes.<sup>1</sup> Therefore improving the stability of BAM is one of the important concerns for the lighting industries.<sup>2,3</sup>

Thermal degradation of this phosphor results from rapid oxidation of europium ions during the heat treatment of the fluorescent lamps. The trivalent europium ions do not fluoresce efficiently in this host. Oxidation of europium ions has been established using x-ray photoemission spectroscopy (XPS), x-ray absorption near-edge structure (XANES), electron spin resonance (ESR), and other methods.<sup>4</sup> It has been speculated that during oxidation, a magnetoplumbite phase containing trivalent europium ions is generated, particularly when excess alumina is present. This conclusion is made possible by comparing x-ray-diffraction patterns of BAM annealed at 1600 °C for an hour and a mixture of BAM and  $\text{EuMgAl}_{11}\text{O}_{19}$  in magnetoplumbite structure.<sup>4</sup> However, BAM apparently degrades when heated in air at 400 °C for

less than an hour. Formation of  $\text{EuMgAl}_{11}\text{O}_{19}$  in the magnetoplumbite structure requires migration of aluminum ions from regions of excess alumina, and also Eu ions from BAM. These processes would very unlikely account for the observed thermal degradation of BAM at temperatures as low as 400 °C.

The crystal structure of BAM is related to the  $\beta$  alumina structure of  $\text{NaAl}_{11}\text{O}_{17}$ .<sup>5</sup> The hexaluminate in both  $\beta$ -alumina, magnetoplumbite, and related phases exhibit layer structures, which consist of the so-called conduction layers containing Ba ions and the spinel blocks stacking alternately along the  $c$  direction (see Fig. 1).<sup>6</sup> In the case of  $\text{BaMgAl}_{10}\text{O}_{17}$ , one  $\text{Al}^{3+}$  ion in the spinel block is replaced by a  $\text{Mg}^{2+}$  ion for charge-compensating the substitution of a  $\text{Na}^+$  ion by a  $\text{Ba}^{2+}$  ion in the conduction plane. The O(5) atoms are the oxygen atoms of the conduction layer. Within the spinel block, the Al(2) (Al-O distances: 1.861–1.881 Å) and Al(3) (Al-O distances: 1.718–1.768 Å) atoms are the tetrahedrally coordinated aluminum ions. The Al(1) (Al-O distances: 1.840–1.980 Å) and Al(4) (Al-O distances: 1.897 Å) are the octahedrally coordinated aluminum ions. It is believed that  $\text{Mg}^{2+}$  ions substitute for tetrahedrally coordinated Al(2) atoms.

BAM is usually synthesized assuming one-to-one substitution of  $\text{Ba}^{2+}$  by  $\text{Eu}^{2+}$ ; yet, the location of  $\text{Eu}^{2+}$  is not precisely known. Multiple sites for europium have been proposed in the literature in order to explain the so-called “green luminescence band.”<sup>7,8</sup> X-ray-diffraction experiments on single crystals in  $\beta'$ -alumina structure have indi-

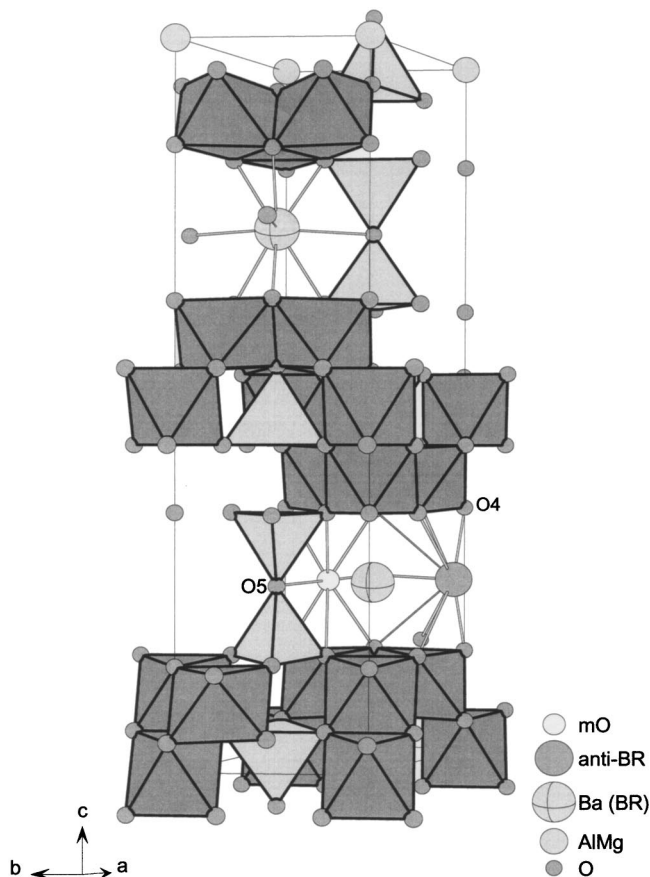


FIG. 1. Crystal structure of  $\text{BaMgAl}_{10}\text{O}_{17}$ . The Beavers-Ross (BR), mid-oxygen (mO), and anti-Beavers-Ross (*a*-BR) are indicated. O(5) refers to oxygen atoms in the intermediate plane. The need for relaxation of O(4) to accommodate a divalent europium ion at the *a*-BR site is discussed in Ref. 24.

cated three sites for  $\text{Eu}^{2+}$ , two being close to the anti-Beavers-Ross site (*a*-BR) and one at the mid-oxygen site (mO).<sup>9</sup> Recent neutron-diffraction measurements on BAM place the  $\text{Eu}^{2+}$  ions near the anti-Beavers Ross site.<sup>10</sup> Optical measurements lead to two different conclusions. Matsui *et al.*<sup>11</sup> concluded that there is only one luminescent center in BAM structure but three different sites were proposed for  $\text{Eu}^{2+}$  in  $\text{SrMgAl}_{10}\text{O}_{17}$ . Our studies on BAM doped with  $\text{Sm}^{2+}$  clearly showed the presence of more than one site.<sup>3</sup> However, clear evidence for multiple sites comes from  $^{151}\text{Eu}$  Mössbauer measurements. Cohen, Remeika, and West proposed two sites, “A” and “B,” for Na  $\beta$ -alumina doped with  $\text{Eu}^{2+}$  prepared by ion exchange method.<sup>12</sup> The A site is a typical  $\text{Eu}^{2+}$  site in oxygen environment but the B site with the smaller isomer shift ( $-14.6$  mm/s) is suggested to represent a roomy site with more diffused 5s wave function. Later Mössbauer measurements<sup>13</sup> on BAM indicated similar possibilities but no detailed line-shape analysis of Mössbauer line shapes taking into account both quadrupolar and/or magnetic broadening was provided to support these conjectures.

$^{151}\text{Eu}$  Mössbauer spectroscopy is an ideal method to probe the oxidation state and local environment of the activator ions. Unlike electron spin resonance that cannot be used for trivalent europium ions, information about both ox-

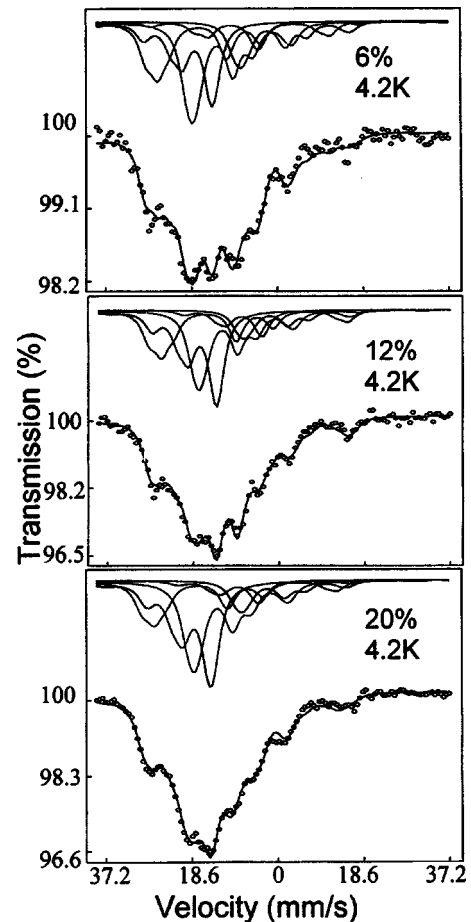


FIG. 2.  $^{151}\text{Eu}$  Mössbauer spectra of three BAM samples containing 6%, 12%, and 20% Eu, respectively.

idation states of europium ions emerges directly from the chemical shift of the nucleus. It is precisely for this reason we employed this technique to probe the locations and electronic structures of europium ions in BAM.

In the present work, we have examined the Mössbauer line shapes of BAM with varying concentrations of europium ions in a variety of conditions of synthesis. We have also investigated the site distribution of  $\text{Eu}^{2+}$  ions in a related hexaluminate,  $\text{Ba}_{.75}\text{Al}_{11}\text{O}_{17.25}$  (phase I),<sup>14–16</sup> which is often considered to form solid solution with BAM. Three oxidized samples were also investigated to determine how various sites are affected during the oxidation process.

## II. EXPERIMENT

$^{151}\text{Eu}$  Mössbauer spectroscopy measurements with the 21.64-keV gamma rays made use of  $^{151}\text{Sm}$  with a half-life of 87 years in  $\text{SmF}_3$  matrix (emitter) and a thin NaI scintillation counter. The Eu doped phosphor (absorber) and the emitter both were cooled to 4.2 or 78 °K in an exchange gas liquid-helium dewar. Standard transmission measurements using a constant acceleration drive were performed.

In general the spectra revealed significant hyperfine structure (Fig. 2). The observed line shapes were analyzed in terms of a superposition of multiple sites, with each site

composed of an 8-line pure quadrupolar pattern characteristic of the  $7/2^+ \rightarrow 5/2^+$  spin sequence. The quadrupolar pattern was parametrized in terms of the nuclear quadrupole coupling  $e^2QV_{zz}$ , isomer shift ( $\delta$ ), asymmetry parameter of the electric field gradient ( $\eta$ ), and linewidth ( $\Gamma$ ). In general, to deconvolute the observed line shape a minimum of five or more sites were found necessary for the results obtained at both 4.2 and at 78 K. The justification for following this procedure of data analysis is addressed in the next section.

### III. ANALYSIS OF MÖSSBAUER LINE SHAPES: THEORETICAL CONSIDERATIONS

Mössbauer spectra at 4.2 K of BAM samples containing 6%, 12%, and 20% Eu are shown in Fig. 2. The broad spectrum spanning over  $\pm 40$  mm/sec consists of at least eight lines. The observed Mössbauer line shape cannot be explained without assuming multiple sites of Eu in the BAM lattice.

In order to understand the line shape of the Mössbauer spectrum, one needs to understand the nature and origin of both electrostatic and magnetic nuclear hyperfine interactions, describing the interactions of the electrons with the nuclei. The Hamiltonian describing this interaction in the absence of any external field is given by<sup>17</sup>

$$H = H_{IS} + H_Q + H_M, \quad (1)$$

where  $H_{IS}$ ,  $H_Q$ , and  $H_M$  describe isomer shift, nuclear quadrupole interaction, and magnetic hyperfine interaction, respectively.

Isomer shift (IS) makes the dominant contribution to the center shift of the mean absorption energy with respect to the emission energy of the Mössbauer active nuclei. This shift, unique to Mössbauer spectroscopy, arises from the finite size of the nucleus, and results from the monopole term from the Coulomb interaction of the nuclear and electronic charge distributions. It is proportional to both the difference of the square of radii of the nucleus in the ground and excited states, and to the difference in the electron density at the nucleus between the source  $A$  and the absorber  $B$ . The isomer shift is given by<sup>18</sup>

$$IS = \frac{2\pi c}{3E_\gamma} Z e^2 [\rho_A(0) - \rho_B(0)] \Delta \langle r_n^2 \rangle, \quad (2)$$

where  $E_\gamma$  is the  $\gamma$ -ray energy,  $Z$  is the nuclear charge,  $\rho_A(0)$  and  $\rho_B(0)$  are the electron charge densities at the nuclei of the source and the absorber, respectively, and  $\Delta \langle r_n^2 \rangle$  is the change in the mean-square charge radius between the excited and ground state. The expression for IS can be simplified to a form

$$IS = \beta \Delta \rho(0) \Delta \langle r_n^2 \rangle, \quad (3)$$

where IS is in mm/s,  $\beta$  in  $\text{fm}^{-2} a_0^3$  mm/s,  $\Delta \rho(0)$  in  $a_0^{-3}$ , and  $\Delta \langle r_n^2 \rangle$  in  $\text{fm}^2$ . For  $^{151}\text{Eu}$  nuclei,  $\beta$  and  $\Delta \langle r_n^2 \rangle$  are  $17.7 \text{ fm}^{-2} a_0^3$  mm/s and  $19.2 \times 10^{-3} \text{ fm}^2$ , respectively.<sup>19</sup> Thus increasing charge densities at the nucleus will lead to increase in IS in the case of  $^{151}\text{Eu}$  Mössbauer spectroscopy. Using a value

of  $-39.02957 a_0^{-3}$  for the change in charge density at the nucleus of a divalent europium ion with respect to a trivalent ion,<sup>18</sup> IS shift for a divalent ion is expected to be approximately  $-13.26$  mm/s. This is indeed where the resonance is usually observed for divalent ions with respect to a source containing trivalent ions as in  $\text{SmF}_3$ .

$H_Q$  describes interaction of the quadrupole moment of the nucleus with the field gradient at the nuclear site and is given by

$$H_Q = \frac{e^2 q Q}{4I(2I-1)} [3I_z^2 - I(I+1) + \eta(I_x^2 - I_y^2)], \quad (4)$$

where  $eq$  and  $\eta$  denote electric-field gradient and asymmetry parameter in the principal coordinate system, respectively, and  $I$  and  $eQ$  denote nuclear spin and quadrupole moment, respectively. Similar to IS, the form of this interaction is derived from the Coulomb interaction of the nuclear charge density with the electronic charge distribution. This interaction being electrostatic in origin cannot remove the Kramer's degeneracy and would lead to an eight line pattern in the case of  $7/2 \rightarrow 5/2$  transition of  $^{151}\text{Eu}$  nuclei.

A magnetically split spectrum results if there is an effective magnetic field at the nuclear site,

$$H_M = -\gamma_N \hbar \mathbf{I} \cdot \mathbf{B}_{\text{eff}}. \quad (5)$$

In the absence of external field,  $B_{\text{eff}}$  can arise from two different sources: magnetic hyperfine interaction and exchange field in a magnetically ordered system. At low temperatures, magnetically split Mössbauer spectra have been observed in insulators with dilute magnetic impurities.<sup>20,21</sup> The effective magnetic field is then provided by the magnetic hyperfine interaction:

$$\mathbf{B}_{\text{eff}} = -\frac{1}{\gamma_N \hbar} \vec{A} \cdot \mathbf{S}, \quad (6)$$

where  $\vec{A}$  is a Cartesian tensor of second rank describing magnetic hyperfine interaction, consisting of both contact and dipolar interactions between nucleus and electrons with spins given by  $I$  and  $S$ . In the case of a paramagnetic ion, if the electron spin is defined along the  $Z$  axis,

$$B_{\text{eff}} = -\frac{1}{\gamma_N \hbar} (A_{xz} S_z + A_{yz} S_y + A_{zz} S_z). \quad (7)$$

Depending on the spin relaxation time  $\tau$ , two scenarios may arise. If  $\tau$  is small compared to the time for which hyperfine tensor  $\vec{A}$  will remain constant, i.e.,  $\sim \hbar/A_{ij}$ , the effective field  $\mathbf{B}_{\text{eff}}$  will be determined by average value of  $S_z$ . At high concentrations, and high temperatures, electron spin-spin interaction may completely wash out any magnetic hyperfine interaction. In most cases, this interaction may just broaden the lines obtained from nuclear quadrupole interaction. In the other extreme, when  $\tau$  is larger than  $\sim \hbar/A_{ij}$ , the electron and nuclear spins will be strongly coupled, and the energy levels will be obtained by diagonalizing the spin Hamiltonian. For isotropic hyperfine interaction, the corresponding Hamiltonian is given by  $a \mathbf{I} \cdot \mathbf{S}$  and the Hamiltonian is described by

$$H_M = 1/2a(F^2 - I^2 - S^2), \quad (8)$$

where  $\mathbf{F} = \mathbf{I} + \mathbf{S}$ . However, if there is a preferred spin-polarization axis due to a zero-field splitting, the effect of the internal magnetic field can still be described by Eq. (5). A classic example is that of dilute  $\text{Fe}^{3+}$  in  $\text{Al}_2\text{O}_3$  observed by Wertheim and Remeika.<sup>21</sup>

In the past, reference has been made to the possibility of magnetically broadened line shape for  $^{151}\text{Eu}$  Mössbauer spectrum for  $\text{La}_{1-x}\text{Eu}_x\text{MgAl}_{11}\text{O}_{19}$  ( $x=0.3,1$ ),<sup>22</sup>  $\text{SrAl}_{12}\text{O}_{19}:\text{Eu}$ ,<sup>23</sup> and  $\text{BaMgAl}_{10}\text{O}_{17}:\text{Eu}$ .<sup>13</sup> This is based on the observation that the linewidth increases with decreasing temperature and decreasing concentration. Tronc *et al.*<sup>22</sup> explained the observed spectrum assuming a Hamiltonian  $H = a_{\parallel}I_z S_z$  and that the spectrum consists of four sets of magnetically split lines derived for four Kramers doublets. The calculated value of the hyperfine constant had reasonably good agreement with that obtained from electron spin resonance measurements.

However, we did not observe a noticeable change in linewidth going from 6% to 20% concentration of europium (Fig. 2) nor in the temperature dependence going from 78 to 4.2 K. *A posteriori*, all the spectra could be reasonably explained assuming a pentamodal (or higher) distribution of Eu ions in the BAM lattice, and the large field gradients for the major sites could be reasonably explained using electronic distribution from first-principles calculations.<sup>24</sup> It is possible that magnetic interaction produces only a small effect contributing to the linewidths of the spectra while the nuclear quadrupole interaction contributes to the splitting of the line shape.

In a ferromagnetic material below the Curie temperature, a magnetic ordering can lead to a large exchange field. For example, below 19 K, EuS orders ferromagnetically<sup>25</sup> and the observed Mössbauer spectrum splits into a pattern characteristic of a static magnetic structure of the  $7/2 \rightarrow 5/2$  transition. In such magnetic systems, additional quadrupolar broadening is observed if the magnetic ion is located at a noncubic site. At  $T < T_C$  (19 K), hysteresis loops characteristic of ferromagnetic ordering are observed in EuS in magnetization measurements performed using a vibrating magnetometer. Magnetization measurements on BAM, in sharp contrast, do not reveal evidence of magnetic hysteresis loops characteristic of magnetic ordering at temperatures above  $T > 10$  K.

The observed magnetization  $M(H)$  as a function of applied field in the  $0 < H < 10$  kOe range display a linear dependence. These are characteristic of a relaxing paramagnetic system but not a ferromagnetically ordered material. The observation correlates well with the  $^{151}\text{Eu}$  Mössbauer line shapes that are best understood in terms of quadrupolar effects rather than Zeeman effects. The  $\text{Eu}^{2+}$  spin relaxation times at the low temperatures appear thus not to be slow enough to yield magnetic hyperfine splittings, as observed in the case of  $\text{Al}_2\text{O}_3$  doped with  $\text{Fe}^{3+}$  by  $^{57}\text{mFe}$  Mössbauer spectroscopy.<sup>21</sup>

The dependence of susceptibility of BAM on reciprocal temperature exhibits clearly the paramagnetic nature of the material described by the Curie law (Fig. 3),<sup>26</sup>

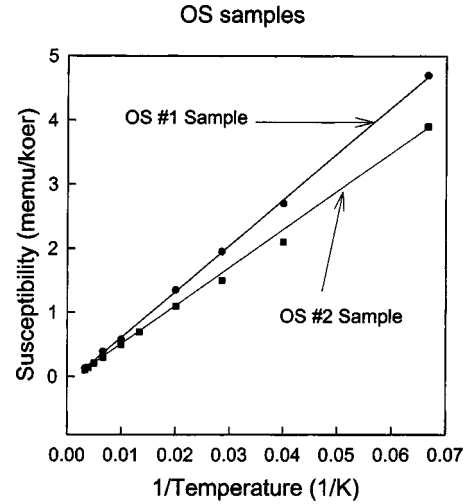


FIG. 3. Variation of susceptibility of two samples of BAM with 12% Eu with respect to temperature. OS #1 and OS #2 correspond to BAM with 12% Eu by Osram Sylvania (OS) before and after oxidation for 40 min.

$$\chi = \frac{Np^2\mu_B^2}{3k_B T}. \quad (9)$$

Using the slope from the linear plot of  $\chi \sim 1/T$  in Fig. 3 and Eq. (9) the effective number of Bohr magnetons was derived to be 6.52. This value may be contrasted to the theoretical value of 7.94 Bohr magnetons for the  $^8S_{7/2}$  ground state given by the equation below:

$$p_{th} = g_j [j(j+1)]^{1/2},$$

$$g_j = 1 + \frac{J(J+1) + S(S+1) - L(L+1)}{2J(J+1)}, \quad (10)$$

where  $g_j$  represents gyromagnetic ratio for the ground state of a divalent europium ion,  $^8S_{7/2}$ . The discrepancy between the observed and theoretical values of effective magnetons is probably related to our assumption that the input concentration of europium ions is the same as the actual contribution, and that all the europium ions exist in a divalent state.

#### IV. EXPERIMENTAL RESULTS AND IDENTIFICATION OF SITES

##### A. Analysis of BAM with 6%, 12%, and 20% Eu

Table I provides a summary of the  $^{151}\text{Eu}$  Mössbauer effect results for BAM samples containing 6%, 12%, and 20% of europium ions (with respect to Ba), respectively. In the fitting procedure, isomer shift (IS), nuclear quadrupole coupling constant ( $e^2qQ$ ), asymmetry parameter ( $\eta$ ), and the linewidth ( $\Gamma$ ), were used as free parameters. The linewidth was assumed to be the same for each site. The distribution of europium ions among various sites has been calculated by assuming that europium ions occupying each site have the same recoil-free fraction at 4.2 K. Using  $\chi^2$  analysis, we observed that a pentamodal distribution of sites with nuclear quadrupolar broadening provides the best fit for the observed

TABLE I.  $^{151}\text{Eu}$  Mössbauer parameters for BAM.

Site	IS (mm/s)	With 6% Eu at 4.2 K		
		$e^2qQ$ (MHz)	$\eta$	% distribution
1	$-18.34 \pm 0.17$	$858.76 \pm 25.22$	0.25	24
2	$-12.08 \pm 0.14$	$-1338.44 \pm 20.08$	0.01	31
3	$-15.63 \pm 0.17$	$-2324.98 \pm 30.77$	0.05	24
4	$-8.64 \pm 0.09$	$1032.60 \pm 75.48$	0.4	6
5	$-0.93 \pm 0.23$	$-1432.57 \pm 43.52$	0.01	15
With 12% Eu at 4.2 K				
Site	IS (mm/s)	$e^2qQ$ (MHz)	$\eta$	% distribution
1	$-17.61 \pm 0.10$	$854.09 \pm 11.98$	0.25	29
2	$-11.50 \pm 0.09$	$-1273.41 \pm 14.08$	0.01	28
3	$-14.25 \pm 0.11$	$-2499.52 \pm 20.94$	0.05	23
4	$-8.69 \pm 0.22$	$1020.07 \pm 43.04$	0.4	9
5	$-0.98 \pm 0.17$	$-1437.50 \pm 33.78$	0.01	11
With 20% Eu at 4.2 K				
Site	IS (mm/s)	$e^2qQ$ (MHz)	$\eta$	% distribution
1	$-18.45 \pm 0.09$	$845.63 \pm 9.82$	0.25	34
2	$-12.22 \pm 0.08$	$-1270.60 \pm 10.99$	0.01	34
3	$-15.67 \pm 0.10$	$-2224.25 \pm 18.87$	0.05	22
4	$-9.16 \pm 0.23$	$1048.28 \pm 45.18$	0.40	7
5	$-1.27 \pm 0.16$	$-1404.09 \pm 30.39$	0.01	3

line shape. Each site contributes 8 Lorentzians with identical linewidths and appropriate branching ratios.

In terms of europium oxidation states, these sites can be classified into three distinct types: sites with divalent europium ions with IS ranging approximately from  $-18$  to  $-11$  mm/s, a site with IS close to  $0.0$  mm characteristic of trivalent europium ions, and a site with IS near  $8.0$  mm/s, intermediate to divalent and trivalent Eu.

### 1. Sites 1, 2, and 3

These sites correspond to europium ions in a divalent state. The range of IS for these sites appear to be very large compared to typical divalent europium ions. Isomer shift of  $-18$  mm/s corresponds to a site with the Eu- $5s$  state being very diffuse as in the “roomy site” originally described by Cohen and Remeika.<sup>12</sup> The other extreme case refers to a situation with IS equal to  $\sim -12$  mm/s which corresponds to an Eu atom located in a very tight environment with increased localization of  $5s$  state and with an increased charge density at the nuclear site.

We have listed in the third and fourth columns values of nuclear quadrupole coupling (NQC) constants and asymmetry parameters. To the best of our knowledge, these are the largest NQC’s reported in the literature to date. For the divalent sites, two of the NQC’s are negative, one (site 2) being close to  $-1300$  MHz and the other (site 3) being close to  $-2324$  MHz. One (site 1) of the NQC’s is positive and approximately close to  $800$  MHz. The asymmetry parameter for this site (site 1) is the largest. The asymmetry parameters are not allowed to vary from sample to sample and have larger uncertainty than other Mössbauer parameters. The largest negative NQC associated with site 3 seemed to change with increasing Eu concentration compared to the other two.

The nearly vanishing values of the asymmetry parameters for the sites 2 and 3 with their negative NQC are consistent with a local structure having a threefold symmetry axis. On the other hand, site 1 with a finite  $\eta$  and a positive NQC represents a site with a local structure having no axial symmetry. BAM crystallizes in the  $P_{6_3/mmc}$  space group. In this

TABLE II.  $^{151}\text{Eu}$  Mössbauer parameters for BAM-Ar at 4.2 K.

Site	IS (mm/s)	$e^2qQ$ (MHz)	$\eta$	% distribution
1	$-18.59 \pm 0.11$	$892.79 \pm 20.75$	0.25	20
2	$-12.02 \pm 0.09$	$-1284.57 \pm 17.29$	0.01	27
3	$-13.66 \pm 0.11$	$-2722.34 \pm 23.71$	0.05	23
4	$-6.74 \pm 0.14$	$1252.48 \pm 28.93$	0.40	16
5	$0.75 \pm 0.07$	$108.72 \pm 0.18$	0.01	14

TABLE III.  $^{151}\text{Eu}$  Mössbauer parameters for BAM-H at 4.2 K.

Site	IS (mm/s)	$e^2qQ$ (MHz)	$\eta$	% distribution
1	$-18.92 \pm 0.11$	$869.39 \pm 14.33$	0.25	26
2	$-12.67 \pm 0.10$	$-1331.06 \pm 15.83$	0.01	26
3	$-14.30 \pm 0.12$	$-2639.95 \pm 21.81$	0.05	24
4	$-8.94 \pm 0.18$	$947.55 \pm 33.41$	0.4	11
5	$-0.72 \pm 0.28$	$-1685.01 \pm 54.72$	0.01	9
6	$0.31 \pm 0.05$	$108.72 \pm 0.35$	0.01	4

space group, there are six special positions with threefold axis:  $2a$ ,  $2b$ ,  $2c$ ,  $2d$ ,  $4e$ , and  $4f$ . The  $2d$  site is occupied by a barium ion,  $2a$  sites by Al(4) ions, and  $2c$  sites by O(5) ions. The “ $2b$ ” site is unoccupied in this  $\beta$ -alumina structure, but it is occupied in the related magnetoplumbite structure. The neutron-diffraction measurements indicate occupancy of this site by  $\text{Eu}^{2+}$  ions in BAM.<sup>10</sup> There exist infinite copies of sites,  $4e$  and  $4f$ , depending on values of  $z$  coordinate. In the limit  $z \rightarrow 0.25$ ,  $4e$  and  $4f$  sites tend to one of the  $2a$ ,  $2b$ ,  $2c$ , and  $2d$  sites. Assuming that the site symmetry of divalent europium ions include a threefold axis, and that it is located close to the intermediate plane,  $2d$  [Beevers-Ross (BR) site:  $(\frac{1}{2}, \frac{2}{3}, \frac{1}{4})$ ],  $2b$  [ $a$ -BR site:  $(0, 0, \frac{1}{4})$ ] or sites close to these two sites are the only plausible locations for divalent europium ions with nearly zero asymmetry parameters.

### 2. Sites 5 (and/or 6)

There are two distinct types of trivalent sites observed in BAM. The Mössbauer parameters of the trivalent ions in oxidized sample are different from that in the pristine samples except for BAM-Ar (Table II). Only in the fresh BAM-H sample (Table III) were both the sites occupied. The trivalent site (site 5) for three phosphor samples in Table I degrades rapidly under oxidation. Emission spectra of  $\text{Eu}^{3+}$  in virgin and oxidized samples also differ in relative intensity of lines at 612 and 618 nm ( $^5D_0 - ^7F_2$ ).

### 3. Site 4

This site with isomer shift of  $\sim -8$  mm/s is a puzzle. Usually, such isomer shifts are observed for europium metal or alloys<sup>27</sup> or europium ions in a mixed-valence configuration.<sup>28</sup> Although BAM is usually prepared in a reducing environment, there is no reason to believe that europium ions are reduced to the metallic state during synthesis.  $\text{Eu}_2\text{O}_3$  is normally used as the source of europium for

BAM. It is usually difficult to reduce  $\text{Eu}^{3+}$  to  $\text{Eu}^{2+}$ . It therefore does not appear plausible that we have metallic europium ions in this large gap oxide.

It is possible that this signal results from a mixed-valence state, the electron transfer between divalent and trivalent ions taking place rapidly compared to the time scale of Mössbauer measurements set by the 10-ns lifetime of the nuclear excited state. The value of the isomer shift is in between divalent europium ( $\sim 13$  mm/s) and trivalent europium ions (0.0 mm/s).<sup>28</sup> This site also disappears readily upon oxidation. However, the persistence of this site at 4.2 K shows that the underlying relaxation process does not slow down enough to observe this signal changing to separate signals from divalent and trivalent ions.

The Mössbauer parameters appear not to change with Eu content of BAM as revealed by our results on samples containing 6%, 12%, and 20% europium ions. Minor changes in site parameters could derive from changes in the local environment of europium ions from samples to samples due to variations in preparation conditions. Occupancy of divalent europium ions among first three sites appears to be the same.

## B. BAM in different synthesis environments

The BAM samples in Table I were synthesized at our phosphor laboratories in Towanda and in Munich using standard procedures. In order to elucidate the role of variations in synthesis conditions, we have also examined two additional phosphor samples, one synthesized in Ar and H atmosphere (BAM-Ar) at OSRAM phosphor facilities at Schwabmünchen, and another sample designated as BAM-H. The latter sample is similar in composition to that used in the neutron-diffraction measurements and was kindly provided by Professor H. T. Hintzen from Technische Universiteit Eindhoven.<sup>10</sup> In Tables II and III, we list the Mössbauer effect parameters for these phosphor samples. In each of these samples, the Mössbauer parameters of sites 1–4 are quite

 TABLE IV.  $^{151}\text{Eu}$  Mössbauer parameters for Ba  $\beta$ -aluminate, phase I, at 4.2 K.

Site	IS (mm/s)	$e^2qQ$ (MHz)	$\eta$	% distribution
1	$-17.33 \pm 0.11$	$825.70 \pm 17.53$	0.25	28
2	$-12.68 \pm 0.12$	$-1041.34 \pm 18.33$	0.01	30
3	$-13.94 \pm 0.14$	$-2622.27 \pm 26.76$	0.05	23
4	$-7.6 \pm 0.15$	$638.48 \pm 25.72$	0.4	17
5	$0.31 \pm 0.06$	$108.86 \pm 45.20$	0.01	2

TABLE V.  $^{151}\text{Eu}$  Mössbauer parameters for BAM with 12% Eu at 4.2 K (40 min oxidation).

Site	IS (mm/s)	$e^2qQ$ (MHz)	$\eta$	% distribution
1	$-17.73 \pm 0.10$	$822.85 \pm 12.78$	0.25	25
2	$-12.28 \pm 0.10$	$-1068.06 \pm 16.10$	0.01	22
3	$-13.52 \pm 0.11$	$-2533.08 \pm 20.61$	0.05	21
4	$-7.99 \pm 0.15$	$863.72 \pm 27.95$	0.4	11
5	$-0.48 \pm 0.32$	$-1472.56 \pm 63.20$	0.01	5
6	$0.65 \pm 0.07$	$178.26 \pm 16.67$	0.01	16

similar to those in the BAM samples discussed earlier. Site 5 for BAM-H is also similar to that of the trivalent site in the BAM samples. For BAM-H, line-shape analysis shows the presence of a new site for  $\text{Eu}^{3+}$  with an IS =  $\sim 0.0$  mm/s. For BAM-Ar, site 5 has parameters closely similar to those of site 6 of BAM-H. It will be shown later that the sixth site most likely represents the site occupied by divalent europium ions after oxidation.

The line-shape parameters for BAM-Ar and BAM-H at 78 K indicate that these parameters do not change appreciably upon increasing the temperature. The occupancy of site 3 changes from 23% to 17% for BAM-Ar, and from 24% to 16% for BAM-H, indicating a lower Debye or vibrational temperature associated this site. The same conclusion can be reached for site 5 associated with  $\text{Eu}^{3+}$  ions in fresh samples of BAM.

### C. Barium hexaaluminate phase I

In Table IV, we list the five site parameters observed in for  $\text{Ba}_{0.75}\text{Al}_{11}\text{O}_{17.25}$  doped with Eu. This material is known as phase I of barium hexaaluminate.<sup>29–31</sup> Phase I is characterized by a highly defective structure containing a Ba vacancy,  $V_{\text{Ba}}$ , one excess oxygen, and no magnesium ions. The accepted structural model describing its charge compensation scheme involves an O ion at an  $m$ -O site forming a Reidinger type of defect,  $V_{\text{Al}}\text{-Al}_i\text{-O}_i\text{-Al}_i\text{-}V_{\text{Al}}$ .<sup>31</sup> The ratio of perfect to defect half cells is 3:1. The defect unit cell contains a perfect half cell and a defect half cell with a Reidinger defect. The half cells are randomly distributed throughout the lattice leaving the space group unchanged. There exists a solid solution regime between BAM and this aluminum rich phase I. It is speculated that the presence of these defect half cells is responsible for degradation of BAM and also the green emission from BAM.

In view of the importance of this phase to understanding of the degradation process of BAM, we chose to investigate this phosphor. We found that the observed line shape can be best fit by five sites, the first four of those having fitting parameters comparable to those of regular BAM (Table I). The trivalent europium ion has the same characteristics as those of the trivalent ions generated through the oxidation process. We did not find any significant difference of the site parameters for BAM and phase I to infer how structural differences contribute to a change in the electronic structure of europium ions in this lattice.

### D. Analysis of thermally degraded samples

Tables V–VII summarize preliminary  $^{151}\text{Eu}$  Mössbauer effect results on thermally degraded BAM samples. Table V lists site parameters for 12% Eu-doped BAM after 40 min of heating at 600 °C in air. Tables VI and VII list site parameters for 20% Eu-doped BAM after heat treatment at 1000 °C of 6 and 12 h, respectively. These site parameters may be compared with those listed in Table I for 12% and 20% Eu-doped BAM samples, respectively.

Our main objective in this study was to understand how various sites degrade upon oxidation and whether such degradation can provide a basis for understanding the loss of luminescence with time due to thermal treatment. So our primary aim is to obtain a quantitative estimate of distribution of europium ions among various sites in both fresh and degraded samples. We assumed that all the five sites present in virgin samples (Tables I, first two parts) are also present in these degraded samples, and an additional site with europium ions in trivalent state results from the oxidation process. Therefore all the spectral analyses are performed assuming a hexamodal distribution of sites with identical recoilless fractions. Since the measurements are done at 4.2 K, the last assumption is not very severe. The main problem is associ-

TABLE VI.  $^{151}\text{Eu}$  Mössbauer parameters for BAM with 20% Eu at 4.2 K (6 h of oxidation).

Site	IS (mm/s)	$e^2qQ$ (MHz)	$\eta$	% distribution
1	$-18.46 \pm 0.06$	$846.04 \pm 2.71$	0.25	17
2	$-12.24 \pm 0.04$	$-1272.74 \pm 4.08$	0.01	15
3	$-15.64 \pm 0.05$	$-2440.60 \pm 7.82$	0.05	9
4	$-9.20 \pm 0.3$	$1056.30 \pm 3.38$	0.40	<1
5	$-1.26 \pm 0.01$	$-1404.63 \pm 4.50$	0.01	<1
6	$-0.23 \pm 0.01$	$108.72 \pm 0.34$	0.01	58

TABLE VII.  $^{151}\text{Eu}$  Mössbauer parameters for BAM with 20% Eu at 4.2 K (12 h oxidation).

Site	IS (mm/s)	$e^2qQ$ (MHz)	$\eta$	% distribution
1	$-18.46 \pm 0.06$	$846.04 \pm 2.71$	0.25	5
2	$-12.24 \pm 0.04$	$-1272.74 \pm 4.08$	0.01	16
3	$-15.64 \pm 0.05$	$-2440.60 \pm 7.82$	0.05	11
4	$-9.20 \pm 0.3$	$1056.30 \pm 3.38$	0.40	<1
5	$-1.26 \pm 0.01$	$-1404.63 \pm 4.50$	0.01	<1
6	$-0.23 \pm 0.01$	$32.62 \pm 0.10$	0.01	68

ated with four sites with divalent ions that are being rapidly oxidized. This makes the fitting procedure very unstable when all the fitting parameters are allowed to vary. Therefore hyperfine interaction parameters for the first five sites were held constant during the fitting procedure.

First we examine the new site that develops during the oxidation process. The isomer shift for this site shifts towards zero compared to the trivalent site that is originally present. It is also interesting to note that the original fifth site and also the fourth site, which we believe to be a mixed valent state, disappear from the 20% samples after 6 h of oxidation. After only 40 min of oxidation, the population of site 5 drops to 50% of its value for the 12% sample (Table V). We also find from luminescence measurements that the trivalent site generated due to oxidation during the thermal treatment of phosphor in air is distinct from those present in virgin phosphors.

## V. CONCLUSION

$^{151}\text{Eu}$  Mössbauer spectroscopy results on BAM phosphor show a pentamodal distribution of Eu sites in the fresh materials. Three of the sites are shown to be occupied by divalent Eu ions. The fourth site most likely corresponds to an Eu ion in a mixed-valence state and the fifth to a site occupied by a trivalent europium ion. Upon oxidation, we observe a sixth site whose parameters are closely similar to those of  $\text{Eu}^{3+}$  in  $\text{EuF}_3$ . Luminescence spectra from the BAM sample before and after oxidation suggest the presence of two different types of  $\text{Eu}^{3+}$  ions in BAM.<sup>32</sup> Upon oxidation of these samples, the  $\text{Eu}^{3+}$  signal observed in virgin BAM samples is rapidly converted to that with IS comparable to that of  $\text{Eu}^{3+}$  in  $\text{EuF}_3$ . The mixed-valence site also disappears with oxidation.

We have made tentative identification of these sites by comparing the observed nuclear quadrupole coupling con-

stants with those calculated using first-principles band-structure approach.<sup>24</sup> The first three  $\text{Eu}^{2+}$  sites are identified with *m*-O (site 1), BR (site 2), and *a*-BR (site 3) sites. These assignments appear to be plausible based on the structure of the intermediate plane in the  $\beta$ -alumina lattice. These sites are accessible to europium ions in the conduction plane. Occupancy of these sites in a phosphor is apparently determined by the thermal and compositional history. Results from  $^{151}\text{Eu}$  Mössbauer measurements of alumina rich phase I of Ba  $\beta$ -alumina do not shed any light on its presence in the standard phosphor samples. The magnitude of Mössbauer parameters required explaining the observed line shape are not very distinct from those of regular phosphor samples.

This work establishes clearly that the oxidation of activator ions is the main cause of thermal degradation of BAM. The europium ions at the three divalent sites behave differently under thermal degradation. Populations of divalent europium ions at these sites continue to decrease with increasing time of thermal treatment in air. However, first-principles calculations in Ref. 24 suggest that the activator ions at the *a*-BR site are thermodynamically more stable than those at the other two sites.<sup>24</sup> A detailed picture of how these sites evolve during the thermal treatment in air is being developed by an elaborate study of thermally degraded samples containing 6% Eu using both  $^{151}\text{Eu}$  Mössbauer and luminescence measurements.

## ACKNOWLEDGMENTS

We are thankful to Professor H. T. Hintzen from Technische Universiteit Eindhoven for a sample of BAM phosphor prepared in his laboratory and to Dr. T. Fries for BAM synthesized in Ar and H environment. We also express our grateful acknowledgment to Mr. E. Dale for many helpful discussions.

\*Present address: Nederlandsche Octrooibureau, The Hague, The Netherlands.

<sup>1</sup>For thermal degradation, see S. Oshio, T. Matsuoka, S. Tanaka, and H. Kobayashi, *J. Electrochem. Soc.* **145**, 3903 (1998). The ultraviolet light related degradation results in color shift during lamp life of high output lamps. Degradation during lamp life is also attributed to adsorption of Hg on BAM; see C. R. Ronda, V. U. Weiler, A. Johnen, J. A. F. Peak, and W. M. P. Van Kemenade, *Method of coating a luminescent material*, U.S. Patent No. 5,811,154 (1998).

<sup>2</sup>A. L. Diaz, C. F. Chenot and B. G. DeBoer, *Proceedings of the 19th International Display Research Conference 1999*, p. 65.

<sup>3</sup>A. Ellens, F. Zwaschka, F. Kummer, A. Meijerink, M. Raukas, and K. Mishra, *J. Lumin.* **93**, 147 (2001).

<sup>4</sup>See, for example, S. Oshio, K. Kitamura, T. Nishiura, T. Shigeta, S. Horii, and T. Matsuoka, *National Technical Report* **43**, 181 (1997); also S. Oshio, T. Matsuoka, S. Tanaka, and H. Kobayashi (Ref. 1).

<sup>5</sup>A. F. Wells, *Structural Inorganic Chemistry*, 5th Edition (Oxford University, New York, 1984), p. 598.

- <sup>6</sup>N. Iyi, Z. Inoue, and S. Kimura, *J. Solid State Chem.* **61**, 236 (1986).
- <sup>7</sup>A. L. N. Stevels and A. D. M. Schrame-de Pauw, *J. Lumin.* **14**, 153 (1976).
- <sup>8</sup>C. R. Ronda and B. M. J. Smets, *J. Electrochem. Soc.* **136**, 570 (1989).
- <sup>9</sup>W. Carrillo-Cabrera, J. O. Thomas, and G. C. Farrington, *Solid State Ionics* **18&19**, 645 (1986).
- <sup>10</sup>S. R. Jansen, Ph.D. thesis, Technische Universiteit, Eindhoven, 1998. For more details about materials used in the neutron-diffraction measurements and about synthesis of BAM-H used in this work, see S. R. Jansen, J. M. Migchels, H. T. Hintzen, and R. Metselaar, *J. Electrochem. Soc.* **146**, 800 (1999); H. T. Hintzen, R. Hanssen, S. R. Jansen, and R. Metselaar, *J. Solid State Chem.* **142**, 48 (1999), and references in the thesis.
- <sup>11</sup>H. Matsui, C. N. Xu, T. Watanabe, M. Akiyama, and X. G. Zheng, *J. Electrochem. Soc.* **147**, 4692 (2000).
- <sup>12</sup>R. L. Cohen, J. P. Remeika, and K. W. West, *J. Phys. (France)* **35**, 513 (1974).
- <sup>13</sup>V. Franknoy-Korös, P. Gelencsér, I. Czakó Nagy, and A. Vértes, *Radiochem. Radioanal. Lett.* **44**, 337 (1980).
- <sup>14</sup>A. L. Stevels, *J. Lumin.* **17**, 121 (1978).
- <sup>15</sup>B. M. J. Smets and J. G. Verlijsdonk, *Mater. Res. Bull.* **21**, 1305 (1986).
- <sup>16</sup>M. Göbbels, S. Kimura, and E. Woermann, *J. Solid State Chem.* **136**, 253 (1998).
- <sup>17</sup>A. Abragam and B. Bleaney, *Electron Paramagnetic Resonance of Transition Ions* (Clarendon, Oxford, 1970); N. N. Greenwood and T. C. Gibbs, *Mössbauer Spectroscopy* (Chapman and Hall, London, 1971).
- <sup>18</sup>A. J. Freeman and D. E. Ellis, in *Mössbauer Isomer Shifts*, edited by G. K. Shenoy and F. E. Wagner (North-Holland, Amsterdam, 1978).
- <sup>19</sup>W. L. Gettys and J. G. Stevens, in *Handbook of Spectroscopy*, edited by J. W. Robinson (CRC, Boca Raton, 1981), Vol. 3.
- <sup>20</sup>G. Lang and W. T. Oosterhuis, *J. Chem. Phys.* **51**, 3608 (1969); W. T. Oosterhuis and G. Lang, *Phys. Rev.* **178**, 439 (1969).
- <sup>21</sup>G. K. Wertheim and J. P. Remeika, *Phys. Lett.* **10**, 14 (1964).
- <sup>22</sup>E. Tronc, D. Saber, A. M. Lejus, and D. Vivien, *J. Less-Common Met.* **111**, 327 (1985).
- <sup>23</sup>H. T. Hintzen, C. J. M. Denissen, and H. M. van Noort, *Mater. Res. Bull.* **24**, 247 (1989).
- <sup>24</sup>M. Stephan, P. C. Schmidt, K. C. Mishra, M. Raukas, A. Ellens, and P. Boolchand, *Z. Phys. Chem. (Munich)* **215**, 1397 (2001).
- <sup>25</sup>See, for example, A. A. Gomes, R. Moreira Xavier, and J. Danon, *Chem. Phys. Lett.* **4**, 239 (1969).
- <sup>26</sup>C. Kittel, *Introduction to Solid State Physics* (Wiley, New York, 1976), p. 440.
- <sup>27</sup>C. M. P. Barton and N. N. Greenwood, in *Mössbauer Data Index*, edited by J. G. Stevens and V. E. Stevens (IFI/Plenum, New York, 1975), pp. 395–446.
- <sup>28</sup>F. Grandjean, A. Gerard, J. Hodges, D. J. Braun, and W. Jeitschko, *Hyperfine Interact.* **15/16**, 765 (1983).
- <sup>29</sup>J. Park and A. N. Cormack, *J. Solid State Chem.* **121**, 278 (1996).
- <sup>30</sup>N. Iyi, Z. Inoue, S. Takekawa, and S. Kimura, *J. Solid State Chem.* **52**, 66 (1984).
- <sup>31</sup>W. L. Roth, F. Reidinger, and S. LaPlaca, in *Superionic Conductors*, edited by G. D. Mahan and W. L. Roth (Plenum, New York, 1977), p. 223.
- <sup>32</sup>To be discussed in a separate publication.